3D Dynamic Coverage and Avoidance Control in Power-constrained UAV Surveillance Networks

William Bentz and Dimitra Panagou

Abstract— **This paper considers dynamic coverage control of multiple power-constrained UAVs. The UAVs are deployed to patrol a domain until the entire space has reached a satisfactory level of coverage. This is achieved through the gathering of visual information by a forward-facing camera, modeled as an anisotropic spherical sector. Coverage and collision avoidance guarantees are met through the design of a high-level kinematic hybrid control scheme consisting of a hold state as well as three coverage modes: local, global and scan mode. Energy-aware methods are encoded into the global coverage state to shift the bulk of spatial redistribution onto less constrained agents. The efficacy of this algorithm is presented through simulation.**

I. Introduction

The past decade has seen rapid improvements in the performance of unmanned aerial vehicles (UAVs) and a continued miniaturization of low-cost sensors. Combined, these mobile sensor networks are useful in a wide range of military and civilian applications including: battlefield surveillance, environmental monitoring, traffic surveillance, and search and rescue operations [1], [2]. The increasing desire for autonomy in mobile sensor networks has spurred interests in coverage control–specifically, 3D dynamic coverage control.

Numerous authors have addressed 2D static coverage problems [3]–[5]. These are often referred to as area coverage, k-coverage, or point coverage and the solutions typically concern directing the agents towards the centroids of Voronoi tesselations [6], [7]. A common theme is that each agent seeks to converge upon a fixed position in space to yield satisfactory steady-state coverage.

Dynamic coverage problems traditionally involve short-range sensors traversing a domain to cover all points up to a satisfactory level over time. The 2D case of this problem has been treated extensively in [8]–[10], with the addition of information decay in [11]. The similar 2D persistent coverage problem includes the periodic servicing requirement of discrete points [12], [13].

Static coverage of 3D environments is presented in [14] The authors extend the classic problems of node scheduling and area coverage to a rough terrain modeled after Encanto Park, Phoenix. Furthermore, they present a novel airdrop based deployment strategy designed around potential aircraft flight paths. Sensor locations remain fixed in space in [15], [16]. The authors of [15] derive the optimal configurations of Pan-Tilt-Zoom cameras to maximize coverage, while the authors of [16] utilize isotropic conical sensing models. In [17], the authors explore dynamic coverage control in quasi-3D domains as the agents are tasked to cover the surfaces of non-planar 3-D objects.

WSN's, particularly those in battlefield applications, are often deployed with short notice and may incur unpredicted initial power constraints such as partially charged batteries. Additionally, harsh terrain may hinder individual agent mobility thus further constraining the agent's power source. Thus, it is crucial that coverage control techniques incorporate energy-awareness for the purpose of maximizing the operational life of the entire network. Most previous research into energy-aware coverage control has been restricted to the static case [18] and [5]; however, dynamic formulations were explored in the context of random walk motion in [19].

Full 3D dynamic coverage, in the sense of active exploration of an unknown domain, is relatively unexplored. Additionally, a full treatment of the problem considering the power limitations of individual agents has not been addressed yet, to the best of our knowledge. The novel contributions of this paper will be the derivation of an energy-aware hybrid control strategy which drives the exploration of a 3D domain such that each point is covered up to a satisfactory level over time. This formulation continues the authors' previous work in [20], [21].

This paper is organized as follows: Section II presents the kinematic and sensing models, as well as an overview of the hybrid control strategy. The local coverage and collision avoidance control strategies are derived in Section III. The global coverage and collision avoidance control strategies are derived in Section IV. Section V presents theoretical guarantees with regards to the coverage error convergence. Section VI presents a series of simulations and summarizes the results. Section VII delivers final concluding remarks.

II. Problem Formulation

A. Kinematic and Sensor Models

Consider a network of UAV agents indexed $i \in \{1, ..., N\}$. Each UAV carries a gimbaled sensor with a 180° range of tilt. With the assumption that a low-level stabilizing controller is readily available, we model the motion of the sensor using

William Bentz is with the Department of Aerospace Engineering, University of Michigan, Ann Arbor; wbentz@umich.edu.

Dimitra Panagou is with the Department of Aerospace Engineering, University of Michigan, Ann Arbor; dpanagou@umich.edu.

The authors would like to acknowledge the support of the Automotive Research Center (ARC) in accordance with Cooperative Agreement W56HZV-14-2-0001 U.S. Army TARDEC in Warren, MI and the support by an Early Career Faculty grant from NASAs Space Technology Research Grants Program

3-D rigid body kinematics [22]:

$$\begin{bmatrix}\dot{x}_i\\ \dot{y}_i\\ \dot{z}_i\end{bmatrix} = \begin{bmatrix}\cos\Theta_i\cos\Psi_i & \sin\Phi_i\sin\Theta_i\cos\Psi_i - \cos\Phi_i\sin\Psi_i & \cos\Phi_i\sin\Theta_i\cos\Psi_i + \sin\Phi_i\sin\Psi_i\\ \cos\Theta_i\sin\Psi_i & \sin\Phi_i\sin\Theta_i\sin\Psi_i + \cos\Phi_i\cos\Psi_i & \cos\Phi_i\sin\Theta_i\sin\Psi_i - \sin\Phi_i\cos\Psi_i\\ -\sin\Theta_i & \sin\Phi_i\cos\Theta_i & \cos\Phi_i\cos\Theta_i\end{bmatrix}\begin{bmatrix}u_i\\ v_i\\ w_i\end{bmatrix}, \quad (1)$$

$$\begin{bmatrix}\dot{\Phi}_i\\ \dot{\Theta}_i\\ \dot{\Psi}_i\end{bmatrix} = \begin{bmatrix}1 & \sin\Phi_i\tan\Theta_i & \cos\Phi_i\tan\Theta_i\\ 0 & \cos\Phi_i & -\sin\Phi_i\\ 0 & \sin\Phi_i\sec\Theta_i & \cos\Phi_i\sec\Theta_i\end{bmatrix}\begin{bmatrix}q_i\\ r_i\\ s_i\end{bmatrix}, \quad (2)$$

where $p_i = [x_i \;\; y_i \;\; z_i]^T$ is the position vector of the sensor resolved in the global Cartesian coordinate frame $\mathcal{G}$ with origin $\mathcal{O}$. p_i is assumed to be co-located with the UAV's center of gravity. $\Omega_i = [\Phi_i \;\; \Theta_i \;\; \Psi_i]^T$ is the 3-2-1 Euler angle vector of the sensor's body fixed frame, $\mathcal{B}_i$ with origin p_i, relative to $\mathcal{G}$. It is assumed that $\mathcal{B}_i$ coincides with the UAV's body-fixed frame when the sensor is gimbaled to a zero-tilt angle (i.e., $\Theta_i \approx 0$ assuming small angles for UAV roll and pitch during flight). The linear velocities $[u_i \;\; v_i \;\; w_i]^T$ and angular velocities $[q_i \;\; r_i \;\; s_i]^T$ are both presented in $\mathcal{B}_i$. The state vector of agent i is defined as $q_i = [p_i^T \;\; \Omega_i^T]^T$. In the sequel, the rotation matrices of (1) and (2) shall be denoted $\mathcal{R}_1$ and $\mathcal{R}_2$ respectively. The agents are confined to a stationary cube domain, $\mathcal{D} \subset \mathbb{R}^3$, which must be fully surveyed.

Agent i's gimbaled sensor is forward facing along the UAV when at a zero tilt angle and has a footprint that shall be referred to as $\mathcal{S}_i$. A spherical sector model is chosen for $\mathcal{S}_i$ as it is representative of the space typically observable to a single camera lens. This model builds upon our previous work in [20] and [21] by rotating the 2-D sensing footprint a magnitude of 180° about its center line. $\mathcal{S}_i$ provides anisotropic sensing data which degrade in quality towards the periphery of the footprint in a similar manner to that of a camera lens. This is encoded through the definition of the following sensing constraint functions for each agent i:

$$c_{1i} = R_i^2 - (\tilde{x} - x_i)^2 - (\tilde{y} - y_i)^2 - (\tilde{z} - z_i)^2, \quad (3a)$$
$$c_{2i} = \alpha_i - \phi_i, \quad (3b)$$
$$c_{3i} = \alpha_i + \phi_i, \quad (3c)$$

where R_i is the sensing range, $\tilde{p}_i = [\tilde{x} \;\; \tilde{y} \;\; \tilde{z}]^T$ is the position of a point within $\mathcal{S}_i$ with respect to $\mathcal{G}$, α_i is the angle between the periphery and centerline of the spherical sector (the $\hat{x}_{\mathcal{B}_i}$ axis), and ϕ_i is the angle between $r_{\tilde{p}_i/p_i} = \tilde{p}_i - p_i$ (resolved in $\mathcal{G}$ by construction) and the $\hat{x}_{\mathcal{B}_i}$ axis. $\phi_i \in [0, \pi]$ is the inverse cosine of the dot product of $\hat{r}_{\tilde{p}_i/p_i}$ and $\hat{x}_{\mathcal{B}_i}$ resolved in $\mathcal{G}$:

$$\phi_i = \arccos\left(\hat{r}_{\tilde{p}_i/p_i} \cdot \hat{x}_{\mathcal{B}_i}|_{\mathcal{G}}\right). \quad (4)$$

Note that:

$$\hat{r}_{\tilde{p}_i/p_i} = \frac{1}{\sqrt{(\tilde{x} - x_i)^2 + (\tilde{y} - y_i)^2 + (\tilde{z} - z_i)^2}}\begin{bmatrix}(\tilde{x} - x_i)\\ (\tilde{y} - y_i)\\ (\tilde{z} - z_i)\end{bmatrix},$$

and $\hat{x}_{\mathcal{B}_i}|_{\mathcal{G}}$ is determined by multiplying $\mathcal{R}_1$ by $[1 \;\; 0 \;\; 0]^T$:

$$\hat{x}_{\mathcal{B}_i}|_{\mathcal{G}} = \begin{bmatrix}\cos\Psi_i\cos\Theta_i\\ \sin\Psi_i\cos\Theta_i\\ -\sin\Theta_i\end{bmatrix}.$$

Agent i is thus capable of detecting objects that lie within an angle of $2\alpha_i > 0$ about the $\hat{x}_{\mathcal{B}_i}$ axis and a range of $R_i > 0$. For the purpose of defining collision avoidance in the sequel, assume that the body of agent i may be bounded with a sphere of radius r_i centered at p_i. This model for agent i is depicted in Fig. 1.

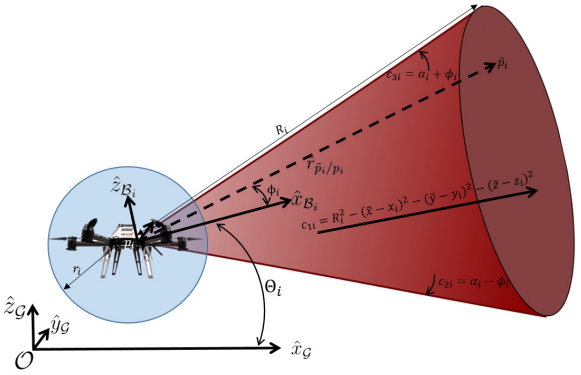

Fig. 1. Agent i is bounded by a sphere of radius r_i and has a forward facing sensor footprint, $\mathcal{S}_i$.

Let us define the barrier function in terms of the sensing constraint functions:

$$B_i = \frac{1}{\max\{0, c_{1i}\}} + \frac{1}{\max\{0, c_{2i}\}} + \frac{1}{\max\{0, c_{3i}\}},$$

and denote $\max\{0, c_{ki}\} = C_{ki}$. One can define the sensing function that represents the quality of information available at each point over the sensing domain as:

$$S_i(q_i, \tilde{p}) = \frac{1}{B_i} = \frac{C_{1i}C_{2i}C_{3i}}{C_{2i}C_{3i} + C_{1i}C_{3i} + C_{1i}C_{2i}}, \quad (5)$$

which takes a value of zero outside of $\mathcal{S}_i$. Define the coverage level provided by agent i at time t as:

$$Q_i(t, \tilde{p}) = \int_0^t S_i\left(q_i(\tau), \tilde{p}\right) d\tau. \quad (6)$$

This summed over all agents produces the global coverage level:

$$Q(t, \tilde{p}) = \sum_{i=1}^{N} Q_i(t, \tilde{p}). \quad (7)$$

Remark 1: In this work, coverage refers to the accumulation of sensing data over time. The effect of agent i's motion is to vary the points $\tilde{p} \in \mathcal{D}$ for which $S_i(q_i, \tilde{p})$ is nonzero. $\mathcal{D}$, is said to be fully covered at a final time t_f when $Q(t_f, \tilde{p}) \geq C^\star$, $\forall \tilde{p} \in \mathcal{D}$ where $C^\star$ is a predefined desired coverage level. Full coverage is achieved by driving the global coverage error, which shall be defined in (8), to zero.

Remark 2: Two agents i and j are said to be collision-free so long as $\|p_i(t) - p_j(t)\| > r_i + r_j$, $\forall t$.

The purpose of this work is to develop and demonstrate techniques that will achieve the goals of *Remark 1* and *Remark 2*. This will require the use of three unique modes of operation, Local Coverage Mode, Global Coverage Mode, and Scan Coverage Mode as well as a hold state which shall be elaborated upon in the following sections.

B. Hybrid Formulation

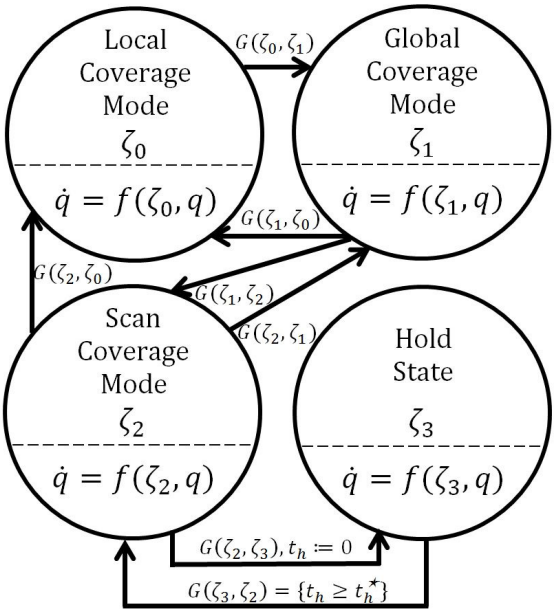

Fig. 2. Agent i operates in accordance with this automaton. For clarity, clock-based transitions are shown explicitly.

The coverage strategy for agent i is represented by the hybrid automaton in Fig. 2, described by the following entities [23]:

- A set of discrete states: $Z_i = \{\zeta_{i0}, \zeta_{i1}, \zeta_{i2}, \zeta_{i3}\}$,
- A set of continuous states: $q_i = \{x_i, y_i, z_i, \Phi_i, \Theta_i, \Psi_i\}$,
- A vector field:
  $f(\zeta_{i0}, q_i) = \mathcal{R}\left[\acute{u}_i^{loc}\ \acute{v}_i^{loc}\ \acute{w}_i^{loc}\ 0\ \acute{r}_i^{loc}\ \acute{s}_i^{loc}\right]^T$,
  $f(\zeta_{i1}, q_i) = \mathcal{R}\left[u_i^{glo}\ v_i^{glo}\ w_i^{glo}\ q_i^{glo}\ r_i^{glo}\ s_i^{glo}\right]^T$,
  $f(\zeta_{i2}, q_i) = \mathcal{R}\left[0\ 0\ 0\ q_i^{scn}\ r_i^{scn}\ s_i^{scn}\right]^T$, and
  $f(\zeta_{i3}, q_i) = \mathcal{R}\left[0\ 0\ 0\ 0\ 0\ 0\right]^T$ where $\mathcal{R} = \begin{bmatrix}\mathcal{R}_1 & 0\\ 0 & \mathcal{R}_2\end{bmatrix}$,
- A set of initial states: $\{\zeta_{i0}\} \times \{q_i \in \mathbb{R}^6 \mid \|p_i\| \leq R_{\mathcal{D}} \wedge \Phi_i \in [-\pi, +\pi] \wedge \Theta_i \in \left[\frac{-\pi}{2}, \frac{+\pi}{2}\right] \wedge \Psi_i \in [-\pi, +\pi]\}$,
- A domain: $Dom\left(\zeta_{ik}\right) = \{q_i \in \mathbb{R}^6\},\ \forall k \in \{1, ..., 4\}$,
- A set of edges: $E = \{(\zeta_{i0}, \zeta_{i1}), (\zeta_{i1}, \zeta_{i0}), (\zeta_{i1}, \zeta_{i2}), (\zeta_{i2}, \zeta_{i0}), (\zeta_{i2}, \zeta_{i1}), (\zeta_{i2}, \zeta_{i3}), (\zeta_{i3}, \zeta_{i2})\}$,
- A guard condition:
  $G\left(\zeta_{i0}, \zeta_{i1}\right) = \{q_i \in \mathbb{R}^6 \mid |\hat{e}_i(t)| < \varepsilon_1\}$,
  $G\left(\zeta_{i1}, \zeta_{i0}\right) = \{q_i \in \mathbb{R}^6 \mid \left(|\hat{e}_i(t)| \geq \varepsilon_1 \wedge \|p_i - p_{\star,i}\| < \varepsilon_2 \wedge \|\Omega_i - \Omega_{\star,i}\| < \varepsilon_3\right)\}$,
  $G\left(\zeta_{i1}, \zeta_{i2}\right) = \{q_i \in \mathbb{R}^6 \mid \left(|\hat{e}_i(t)| < \varepsilon_1 \wedge \|p_i - p_{\star,i}\| < \varepsilon_2 \wedge \|\Omega_i - \Omega_{\star,i}\| < \varepsilon_3\right)\}$,
  $G\left(\zeta_{i2}, \zeta_{i0}\right) = \{q_i \in \mathbb{R}^6 \mid \left(|\hat{e}_i(t)| \geq \varepsilon_1 \wedge \|p_i - p_{\star,i}\| < \varepsilon_2 \wedge \|\Omega_i - \Omega_{\star\star,i}\| < \varepsilon_3\right)\}$,
  $G\left(\zeta_{i2}, \zeta_{i1}\right) = \{q_i \in \mathbb{R}^6 \mid \left(|\hat{e}_i(t)| < \varepsilon_1 \wedge \hat{C}_i^{\tilde{j}} = \infty \wedge \|p_i - p_{\star,i}\| < \varepsilon_2 \wedge \|\Omega_i - \Omega_{\star\star,i}\| < \varepsilon_3\right)\}$,
  $G\left(\zeta_{i2}, \zeta_{i3}\right) = \{q_i \in \mathbb{R}^6 \mid \left(|\hat{e}_i(t)| < \varepsilon_1 \wedge \hat{C}_i^{\tilde{j}} \neq \infty \wedge \|p_i - p_{\star,i}\| < \varepsilon_2 \wedge \|\Omega_i - \Omega_{\star\star,i}\| < \varepsilon_3\right)\}$,
  $G\left(\zeta_{i3}, \zeta_{i2}\right) = \{t_h \geq t_h^\star\}$,
- A set of clocks: $C = \{t_h\}$ and,
- A reset map: $R\left(\zeta_{i2}, \zeta_{i3}, t_h\right) = \{0\}$, and continuous states do not reset between transitions.

Note that $\hat{e}_i(t)$, shall later be defined in (12). It evolves as a function of the time history of the continuous states and essentially represents how well the local coverage protocol is proceeding. ε_1 is a guard value for $\hat{e}_i(t)$, while ε_2 and ε_3 are guard values for position and orientation errors respectively. $\hat{C}_i^{\tilde{j}}$ shall be defined in (29) and has value ∞ when full coverage has been achieved on subdomain $\mathcal{D}^{\tilde{j}}$ defined Section IV. $\Omega_{\star,i}$ and $\Omega_{\star\star,i}$ are desired orientations that shall be defined in Sections III and IV. The control laws presented in the vector field definition shall be derived in the proceeding three sections.

III. Local Coverage Mode

A. Nominal Control Strategy

Local coverage is the nominal mode that directs active exploration by the agents. Define the global coverage error with respect to $C^\star$ as:

$$E(t) = \int_{\mathcal{D}} h(C^\star - Q(t, \tilde{p}))\, d\tilde{p}, \tag{8}$$

where $h(w) = (\max\{0, w\})^3$ is $\mathcal{C}^2$ and has first derivative $h' = \frac{dh}{dw} = 3(\max\{0, w\})^2$ and second derivative $h'' = \frac{d^2h}{dw^2} = 6(\max\{0, w\})$. This definition for $h(w)$ was chosen to prevent a negative contribution to the coverage error at the points $\tilde{p} \mid Q(t, \tilde{p}) > C^\star$. The nominal control strategy will be derived via differentiation of (8), a volume integral, so a few mathematical preliminaries are required.

Recall the generalized transport theorem [24]:

$$\frac{d}{dt}\int_{R_{(s)}} f dV = \int_{R_{(s)}} \frac{\partial f}{\partial t}\, dV + \int_{S_{(s)}} f \mathbf{v}_{(\mathbf{s})} \cdot \mathbf{n}\, dA \tag{9}$$

where f is any scalar-, vector-, or tensor-valued function of position and time, $S_{(s)}$ is the boundary of the volume $R_{(s)}$ over which f is integrated, $\mathbf{n}$ is the unit vector normal to the boundary, and $\mathbf{v}_{(\mathbf{s})}$ is the velocity of the boundary. V and A refer to volume and area respectively. Invoking (9) allows for differentiation of (8) with respect to time:

$$\begin{aligned}\dot{E}(t) = &\int_{\mathcal{D}} h'(C^\star - Q(t, \tilde{p}))\left(\frac{-\partial Q(t, \tilde{p})}{\partial t}\right) d\tilde{p}\\ &+ \int_{\partial\mathcal{D}} \big(h(C^\star - Q(t, \tilde{p}))\big)\mathbf{v}_{(\mathbf{s})} \cdot \mathbf{n}\, dA,\end{aligned} \tag{10}$$

where $\partial\mathcal{D}$ is the boundary of $\mathcal{D}$. The control volume is $\mathcal{D}$ which is time invariant and thus $\mathbf{v}_{(\mathbf{s})} = 0$. This expression

Expand $\frac{d}{dt}(S_i(q_i(t),\tilde{p}))$:

$$\frac{d}{dt}(S_i(q_i(t),\tilde{p})) = \frac{\partial S_i}{\partial x_i}\dot{x}_i(t) + \frac{\partial S_i}{\partial y_i}\dot{y}_i(t) + \frac{\partial S_i}{\partial z_i}\dot{z}_i(t) + \frac{\partial S_i}{\partial \Psi_i}\dot{\Psi}_i(t) + \frac{\partial S_i}{\partial \Theta_i}\dot{\Theta}_i(t) = \left(\frac{\partial S_i}{\partial x_i}\cos\Theta\cos\Psi + \frac{\partial S_i}{\partial y_i}\cos\Theta\sin\Psi - \frac{\partial S_i}{\partial z_i}\sin\Theta\right)u_i(t)$$
$$+ \left(\frac{\partial S_i}{\partial x_i}(\sin\Phi\sin\Theta\cos\Psi - \cos\Phi\sin\Psi) + \frac{\partial S_i}{\partial y_i}(\sin\Phi\sin\Theta\sin\Psi + \cos\Phi\cos\Psi) + \frac{\partial S_i}{\partial z_i}\sin\Phi\cos\Theta\right)v_i(t)$$
$$+ \left(\frac{\partial S_i}{\partial x_i}(\cos\Phi\sin\Theta\cos\Psi + \sin\Phi\sin\Psi) + \frac{\partial S_i}{\partial y_i}(\cos\Phi\sin\Theta\sin\Psi - \sin\Phi\cos\Psi) + \frac{\partial S_i}{\partial z_i}\cos\Phi\cos\Theta\right)w_i(t)$$
$$+ \left(\frac{\partial S_i}{\partial \Psi_i}\sin\Phi\sec\Theta + \frac{\partial S_i}{\partial \Theta_i}\cos\Phi\right)r_i(t) + \left(\frac{\partial S_i}{\partial \Psi_i}\cos\Phi\sec\Theta - \frac{\partial S_i}{\partial \Theta_i}\sin\Phi\right)s_i(t). \tag{15}$$

Now introduce the following definitions:

$$a_{i0}(t,Q(t,\tilde{p})) = \int_{D_i} h''(C^\star - Q(t,\tilde{p}))S_i(q_i(t),\tilde{p})(S_i(q_i(t),\tilde{p})d\tilde{p}, \tag{16}$$

$$a_{i1}(t,Q(t,\tilde{p})) = \int_{D_i} h'(C^\star - Q(t,\tilde{p}))\left(\frac{\partial S_i}{\partial x_i}\cos\Theta\cos\Psi + \frac{\partial S_i}{\partial y_i}\cos\Theta\sin\Psi - \frac{\partial S_i}{\partial z_i}\sin\Theta\right)d\tilde{p}, \tag{17}$$

$$a_{i2}(t,Q(t,\tilde{p})) = \int_{D_i} h'(C^\star - Q(t,\tilde{p}))\left(\frac{\partial S_i}{\partial x_i}(\sin\Phi\sin\Theta\cos\Psi - \cos\Phi\sin\Psi) + \frac{\partial S_i}{\partial y_i}(\sin\Phi\sin\Theta\sin\Psi + \cos\Phi\cos\Psi) + \frac{\partial S_i}{\partial z_i}\sin\Phi\cos\Theta\right)d\tilde{p}, \tag{18}$$

$$a_{i3}(t,Q(t,\tilde{p})) = \int_{D_i} h'(C^\star - Q(t,\tilde{p}))\left(\frac{\partial S_i}{\partial x_i}(\cos\Phi\sin\Theta\cos\Psi + \sin\Phi\sin\Psi) + \frac{\partial S_i}{\partial y_i}(\cos\Phi\sin\Theta\sin\Psi - \sin\Phi\cos\Psi) + \frac{\partial S_i}{\partial z_i}\cos\Phi\cos\Theta\right)d\tilde{p}, \tag{19}$$

$$a_{i4}(t,Q(t,\tilde{p})) = \int_{D_i} h'(C^\star - Q(t,\tilde{p}))\left(\frac{\partial S_i}{\partial \Psi_i}\sin\Phi\sec\Theta + \frac{\partial S_i}{\partial \Theta_i}\cos\Phi\right)d\tilde{p}, \tag{20}$$

$$a_{i5}(t,Q(t,\tilde{p})) = \int_{D_i} h'(C^\star - Q(t,\tilde{p}))\left(\frac{\partial S_i}{\partial \Psi_i}\cos\Phi\sec\Theta - \frac{\partial S_i}{\partial \Theta_i}\sin\Phi\right)d\tilde{p}. \tag{21}$$

One can then rewrite (14) as:

$$\dot{\hat{e}}_i(t) = a_{i0}(t,Q(t,\tilde{p})) - u_i(t)a_{i1}(t,Q(t,\tilde{p})) - v_i(t)a_{i2}(t,Q(t,\tilde{p})) - w_i(t)a_{i3}(t,Q(t,\tilde{p})) - r_i(t)a_{i4}(t,Q(t,\tilde{p})) - s_i(t)a_{i5}(t,Q(t,\tilde{p})). \tag{22}$$

---

reduces to:

$$\dot{E}(t) = \int_D h'(C^\star - Q(t,\tilde{p}))\left(\frac{-\partial Q(t,\tilde{p})}{\partial t}\right)d\tilde{p}, \tag{11}$$

which expands to:

$$\begin{aligned}\dot{E}(t) &= -\int_D h'(C^\star - Q(t,\tilde{p}))\sum_{i=1}^{N} S_i(q_i(t),\tilde{p})d\tilde{p} \\ &= -\sum_{i=1}^{N}\int_D h'(C^\star - Q(t,\tilde{p}))S_i(q_i(t),\tilde{p})d\tilde{p} \\ &= \sum_{i=1}^{N}\hat{e}_i(t),\end{aligned} \tag{12}$$

where the definition of $\hat{e}_i(t)$ is implicit. (12) is less than or equal to zero. Therefore, (8) is non-increasing. In fact, $\dot{E}$ may only take zero value at some time $t^\star$ if $\forall i \in N$, $Q(t^\star,\tilde{p}) \geq C^\star\ \forall \tilde{p} \in D \mid S_i(q_i(t^\star),\tilde{p}) > 0$. Moving forward, the strategy will be to design control laws that drive (12) to be increasingly negative. Taking the derivative of (12) with respect to time yields:

$$\ddot{E}(t) = \sum_{i=1}^{N}\dot{\hat{e}}_i(t) \tag{13}$$

following once again from (9). $\dot{\hat{e}}_i(t)$ is defined as:

$$\dot{\hat{e}}_i(t) = -\int_{D_i}\Big(-h''(C^\star - Q(t,\tilde{p}))S_i(q_i(t),\tilde{p})S_i(q_i(t),\tilde{p}) + h'(C^\star - Q(t,\tilde{p}))\frac{d}{dt}(S_i(q_i(t),\tilde{p}))\Big)d\tilde{p}. \tag{14}$$

The sensing footprint is independent of Φ_i assuming that the centerline of the spherical sector is aligned with the $\hat{x}_{\mathcal{B}_i}$ axis. $\frac{d}{dt}(S_i(q_i(t),\tilde{p}))$ is expanded in (15) and through the definitions in (16-21) one may restate (14) as (22). If one were to command zero inputs to this system, it becomes clear that $a_{i0}(t,Q(t,\tilde{p}))$ may be physically interpreted as the rate at which the coverage rate is reducing due to information saturation at any particular position and orientation of the sensing footprint, $\mathcal{S}_i$. As the footprint remains stationary, there are diminishing returns on the value of newly acquired information. Thus, the additional terms in (22) allow for the coverage rate to be increased by mobilizing the sensor. One

strategy is to define the following control law:

$$u_i^{loc} = k_u^{loc}\ a_{i1}(t, Q(t,\tilde{p})), \tag{23a}$$
$$v_i^{loc} = k_v^{loc}\ a_{i2}(t, Q(t,\tilde{p})), \tag{23b}$$
$$w_i^{loc} = k_w^{loc}\ a_{i3}(t, Q(t,\tilde{p})), \tag{23c}$$
$$r_i^{loc} = k_r^{loc}\ a_{i4}(t, Q(t,\tilde{p})), \tag{23d}$$
$$s_i^{loc} = k_s^{loc}\ a_{i5}(t, Q(t,\tilde{p})), \tag{23e}$$

which decreases (22) with the intent of preventing (12) from reaching zero.

B. Collision Avoidance Augmentation

The purpose of this subsection is to encode collision avoidance, as defined in *Definition 1*, directly into the local coverage control strategy (23) through a straightforward modification to the global coverage level (7). We refer to this technique as map augmentation.

Assumption 1: Agent i knows the state q_j of agent j if $\|r_{p_i/p_j}\| = \|p_i - p_j\| \leq R_i$.

Consider agent i which must avoid agent j. Define the buffer distance of i from j as $R_{b,ij} = R_i + r_i + r_j$. Define the coverage map avoidance term:

$$\acute{Q}_{ij}(t,\tilde{p}) = \begin{cases} M_{1i}(p_j,\tilde{p}), & \text{if } \|p_i - p_j\| \leq R_i; \\ 0, & \text{otherwise,} \end{cases} \tag{24}$$

where:

$$M_{1i}(p_j,\tilde{p}) = \begin{cases} C^\star, & \text{if } \tilde{p} \in \bar{B}_{R_{b,ij}}(p_j); \\ 0, & \text{otherwise,} \end{cases} \tag{25}$$

and $\bar{B}_{R_{b,ij}}(p_j)$ is the closed ball of radius $R_{b,ij}$ centered at p_j. $\acute{Q}_{ij}(t,\tilde{p})$ augments the global coverage map for i as follows:

$$\acute{Q}_i(t,\tilde{p}) = Q(t,\tilde{p}) + \sum_{j=1}^{N-1} \acute{Q}_{ij}(t,\tilde{p}). \tag{26}$$

$\acute{Q}_i(t,\tilde{p})$ is the avoidance augmented global coverage map for agent i. This term allows agent i to perceive a closed ball of space around j as fully covered if the agents come into close proximity. This effect is realized by substituting $\acute{Q}_i(t,\tilde{p})$ for $Q(t,\tilde{p})$ in the proposed local coverage control law (23):

$$\acute{u}_i^{loc} = k_u^{loc}\ a_{i1}(t, \acute{Q}_i(t,\tilde{p})), \tag{27a}$$
$$\acute{v}_i^{loc} = k_v^{loc}\ a_{i2}(t, \acute{Q}_i(t,\tilde{p})), \tag{27b}$$
$$\acute{w}_i^{loc} = k_w^{loc}\ a_{i3}(t, \acute{Q}_i(t,\tilde{p})), \tag{27c}$$
$$\acute{r}_i^{loc} = k_r^{loc}\ a_{i4}(t, \acute{Q}_i(t,\tilde{p})), \tag{27d}$$
$$\acute{s}_i^{loc} = k_s^{loc}\ a_{i5}(t, \acute{Q}_i(t,\tilde{p})), \tag{27e}$$

where $a_{ik}(t, \acute{Q}_i(t,\tilde{p})), \forall k \in \{1,...,5\}$, are functions of $\acute{Q}_i(t,\tilde{p})$ rather than $Q(t,\tilde{p})$.

Theorem 1: Assuming both agents are operating under the control law (27), agent i may not collide with agent j.

Proof: Note that in (17), (18), (19), (20), and (21), each additive term under the integral sign is multiplied by some derivative of $S_i(q_i,\tilde{p})$. Recall from Section II that $S_i(q_i,\tilde{p})$ is identically zero outside of $\mathcal{S}_i$. Therefore, (17), (18), (19), (20), and (21) may be equivalently integrated over $\mathcal{S}_i$ instead of $\mathcal{D}$. This holds true also for the augmented forms in (27). As $\|p_i - p_j\|$ approaches $(r_i + r_j)$, $M_{1i}(p_j,\tilde{p})$ is defined as $C^\star$, $\forall \tilde{p} \in \mathcal{S}_i$ and $\acute{Q}_i(t,\tilde{p}) \geq C^\star$, $\forall \tilde{p} \in \mathcal{S}_i$. Thus $\lim_{\|p_i - p_j\| \to (r_i + r_j)} a_{ik}(t, \acute{Q}_i(t,\tilde{p})) = 0, \forall m \in \{1,...,5\}$. Therefore, (27) decay to zero as $\|p_i - p_j\| \to (r_i + r_j)$. Agent i is comes to rest in this limit (as does agent j which can be demonstrated through the same logic). Agent i and j avoid collision by *Remark 2*. This concludes the proof. ■

This theoretical guarantee is made with respect to a worst case scenario in which the agents come to rest adjacent to one another. This can only occur if the agents' local space has reached a full coverage level. The two agents would then switch into global coverage mode and make use of the global coverage collision avoidance technique presented in Section IV. Under nominal circumstances, the natural motion of the agents under (27) would rarely lead to this scenario. Rather, any portion of $\mathcal{S}_i$ which extends outside of $\bar{B}_{R_{b,ij}}(p_j)$ into a portion of $\mathcal{D}$ not fully covered would tend to direct i away from j.

IV. Global Coverage Mode

A. Subdomain Partitioning

The local coverage strategy is limited in that its control laws (27) decay to zero when $\acute{Q}_i(t,\tilde{p}) \geq C^\star$, $\forall \tilde{p} \in \mathcal{S}_i$. Essentially, if the immediate surroundings of agent i are fully covered, the agent would stop moving. Our energy-aware global coverage mode prevents this scenario by redirecting such agents toward waypoints in less covered portions of the domain. This mode is initiated for agent i when:

$$|\hat{e}_i(t)| < \varepsilon_1, \tag{28}$$

that is, agent i's contribution to the rate of change of (8) has dropped below a predefined threshold ε_1. At this point, $\mathcal{D}$ is divided into an $n \times n \times n$ grid of subdomains $\mathcal{D}^j$, $\forall j \in \{1,...,n^3\}$. Each $\mathcal{D}^j$ should be a cube of dimension $\ell \times \ell \times \ell$ for $\ell < \sqrt{2}R_i$, and the possible waypoints W^j placed at the centroid of each $\mathcal{D}^j$. This grid size guarantees that for any point within the domain, a centroid and orientation exists that will place the point within $int\,(\mathcal{S}_i)$.

We define the following function to encode the anticipated local coverage error for agent i in each subdomain $\mathcal{D}^j$:

$$\hat{C_i^j}(t_{gc}) = \int_{\mathcal{D}^j} \min\{C^\star, \acute{Q}_i(t_{gc},\tilde{p})\} d\tilde{p} + \delta\left(C^\star V_{\mathcal{D}^j} - \int_{\mathcal{D}^j} \min\{C^\star, \acute{Q}_i(t_{gc},\tilde{p})\} d\tilde{p}\right), \tag{29}$$

where $V_{\mathcal{D}^j} = \ell^3$ is the volume of each $\mathcal{D}^j$, $\delta(w)$ is the dirac delta function defined such that $\delta(0) = \infty$ and $\delta(w) = 0$, $\forall w \neq 0$, and t_{gc} is the time at which global coverage mode was initiated. (29) is the coverage weight of each subdomain $\mathcal{D}^j$ and is defined as ∞ if the coverage level reaches at least $C^\star$ on every point in $\mathcal{D}^j$. This is accomplished with a dirac delta function which ensures that fully covered subdomains shall not be selected as waypoints. The arguments of the minimum functions prevent discrete

points covered well beyond $C^\star$ from carrying an unwarranted weight. Such a scenario may result in patches of gross coverage levels producing subdomain coverage levels in excess of $C^\star V_{\mathcal{D}^j}$ while discrete points $\tilde{p} \in \mathcal{D}^j$ remain uncovered.

B. Energy-aware Waypoint Selection

Power conservation may be encoded into the global coverage strategy by considering the relative distances of W_j from the agent. Define the actuation accumulation function:

$$\Gamma_i(t_{gc}) = \int_0^{t_{gc}} \gamma_{i1}|u_i(\tau)| + \gamma_{i2}|v_i(\tau)| + \gamma_{i3}|w_i(\tau)| + \gamma_{i4}|r_i(\tau)| + \gamma_{i5}|s_i(\tau)|d\tau \quad (30)$$

which represents the net accumulated actuator effort since deployment. $\gamma_{ik} > 0$, $\forall k \in \{1, ..., 5\}$ are cost weights that can be assigned based upon a particular system's rate of energy usage. (29) and (30) can be combined into the overall cost definition:

$$\tilde{j} = \underset{j \in \{1,\dots,n^3\}}{\operatorname{argmin}} \left((\Lambda_{i0} + \Gamma_i(t_{gc})) \left\| p_i - W^j \right\| + \Lambda_{i1} \hat{C_i^j} \right), \quad (31a)$$

$$p_{\star,i} = W^{\tilde{j}}, \quad (31b)$$

where the chosen waypoint, $p_{\star,i}$, for agent i is assigned to be the centroid of the subdomain indexed by $\tilde{j}$, that minimizes the cost function (31a). $\Lambda_{i0} > 0$ and $\Lambda_{i1} > 0$ are cost weights.

(31a) utilizes a static weight, Λ_{i0}, and a dynamic weight, $\Gamma_i(t_{gc})$, to penalize the selection of waypoints that are spatially distant from the agent's current position. $\Gamma_i(t_{gc})$ grows in time as a function of agent i's actuation effort. This cost is weighted against the relative coverage level of the subdomain. In real world implementation, the value of Λ_{i0} would be assigned upon deployment as a function of agent i's remaining battery life. This offers energy conserving flexibility to scenarios in which a multi-agent sensing network may be deployed with short notice and disparate battery charge levels. γ_{ik}, $\forall k \in \{1, ..., 5\}$, may be increased for individual agents which consume energy at a faster rate. These weights allow for agents with a history of less actuation effort to select more distant waypoints thus reducing the need for persistent spatial relocation of the more power constrained agents.

Upon selecting the waypoint, the agent must determine the optimal orientation to assume at the destination. This orientation will be the one for which $\mathcal{S}_i$ is exposed to the least covered subspace of $\mathcal{D}$, or in other words the solution to the following optimization problem:

$$\Omega_{\star,i} = \arg\max_{\Omega} \left(\int_D h' \left(C^\star - \acute{Q}_i(t_{gc}, \tilde{p}) \right) \left(S_i(q_{\star,i}, \tilde{p}) \right) d\tilde{p} \right), \quad (32)$$

where $q_{\star,i} = \left[{p_{\star,i}}^T \ \Omega_{\star,i}^T \right]^T$. Selecting a destination orientation with the minimum coverage level maximizes (12). This maximizes the initial coverage rate at the completion of global coverage mode. Recall that the centerline of $\mathcal{S}_i$ is aligned with $\hat{x}_{\mathcal{B}_i}$; thus, the choice of $\Phi_{\star,i}$ is arbitrary and we define it as zero assuming small roll angles during quadrotor flight.

C. Waypoint Convergence and Collision Avoidance

Convergence to the desired position, $p_{\star,i}$, as well as collision avoidance are achieved using the following control scheme based upon that presented in [25] and later in [26]. Define a candidate Lyapunov function:

$$\mathcal{V}_{i0} = \|p_i - p_{\star,i}\|^2. \quad (33)$$

which is convex and encodes convergence of agent i to the destination. Now define a global avoidance constraint for each of the $j \neq i$ friendly agents:

$$c_{4ij} = (x_i - x_j)^2 + (y_i - y_j)^2 + (z_i - z_j)^2 - (r_i + r_j)^2 > 0,$$

to encode that collision avoidance requires $\|p_i - p_j\| > r_i + r_j$. Define a logarithmic barrier function in terms of this constraint:

$$b_{ij}(p_i, p_j) = -\ln(c_{4ij}(p_i, p_j)),$$

and define, as in [27], the recentered barrier function which tends to $+\infty$ as $\|p_i - p_j\| \to r_i + r_j$, and to zero as $p_i \to p_{\star,i}$:

$$q_{ij}(p_i, p_j) = b_{ij}(p_i, p_j) - b_{ij}(p_{\star,i}, p_j). \quad (34)$$

To ensure that our Lyapunov function is non-negative everywhere, define:

$$\mathcal{V}'_{ij}(p_i, p_j) = (q_{ij}(p_i, p_j))^2.$$

Recall from *Assumption 1* that agent i knows the state q_j of agent j if $\|p_i - p_j\| \leq R_i$. Therefore, the global avoidance constraint is activated under this condition using a bump function which is $\mathcal{C}^2$ with respect to the agent distance:

$$\sigma_{ij} = \begin{cases} 1 & \text{if } r_i + r_j \leq d_{ij} \leq R_z \\ Ad_{ij}^3 + Bd_{ij}^2 + Cd_{ij} + D & \text{if } R_z < d_{ij} < R_i \\ 0 & \text{if } d_{ij} \geq R_i \end{cases}$$

where $r_i + r_j < R_z < R_i$ and $d_{ij} = \|p_i - p_j\|$. The coefficients are defined as follows: $A = -(2/(R_z - R_i)^3)$, $B = (3(R_z + R_i)/(R_z - R_i)^3)$, $C = (-6R_zR_i/(R_z - R_i)^3)$, and $D = (R_i^2(3R_z - R_i)/(R_z - R_i)^3)$. Therefore, the global avoidance constituent Lyapunov function is:

$$\mathcal{V}_{ij}(p_i, p_j) = \sigma_{ij}\mathcal{V}'_{ij}(p_i, p_j),$$

which augments the candidate Lyapunov function:

$$\nu_i = \mathcal{V}_{i0} + \sum_{j=1,\, j\neq i}^{N} \mathcal{V}_{ij}$$

and may be scaled between zero and one to form our elected Lyapunov function for p_i:

$$\mathcal{V}_i = \frac{\nu_i}{1 + \nu_i}. \quad (35)$$

As discussed in [26] and [25], trajectories that follow the negative gradient of $\mathcal{V}_i$ shall be stabilizing and in-fact almost

globally asymptotically stabilizing. Such a controller may be defined as:

$$\begin{bmatrix} u_i^{glo} \\ v_i^{glo} \\ w_i^{glo} \end{bmatrix} = \mathcal{R}_1^{-1} \begin{bmatrix} \frac{-\partial \mathcal{V}_i}{\partial x_i} \left(\frac{U_{max}}{\sqrt{\left(\frac{\partial \mathcal{V}_i}{\partial x_i}\right)^2 + \left(\frac{\partial \mathcal{V}_i}{\partial y_i}\right)^2 + \left(\frac{\partial \mathcal{V}_i}{\partial z_i}\right)^2}} \right) \\ \frac{-\partial \mathcal{V}_i}{\partial y_i} \left(\frac{U_{max}}{\sqrt{\left(\frac{\partial \mathcal{V}_i}{\partial x_i}\right)^2 + \left(\frac{\partial \mathcal{V}_i}{\partial y_i}\right)^2 + \left(\frac{\partial \mathcal{V}_i}{\partial z_i}\right)^2}} \right) \\ \frac{-\partial \mathcal{V}_i}{\partial z_i} \left(\frac{U_{max}}{\sqrt{\left(\frac{\partial \mathcal{V}_i}{\partial x_i}\right)^2 + \left(\frac{\partial \mathcal{V}_i}{\partial y_i}\right)^2 + \left(\frac{\partial \mathcal{V}_i}{\partial z_i}\right)^2}} \right) \end{bmatrix}. \tag{36}$$

where U_{max} is the maximum linear velocity of the slowest agent in the network.

The anomalous scenario in which multiple agents become isolated in critical points generated by recentered barrier functions (34) is overcome by defining an event in which the motion of multiple agents in the global coverage mode has halted for a predefined period of time. In this scenario, one agent, i_{ld}, is randomly selected as a leader that shall elect Lyapunov function (33) in place of $\mathcal{V}_i$ in (36). Collision avoidance is still guaranteed as the remaining j agents acting under either (36) or (27) shall actively avoid i_{ld}. The leader converges upon its destination and, having disrupted the location of the critical points in space, the remaining agents shall most likely do so as well. Otherwise, the event is retriggered.

Convergence to the desired orientation, $\Omega_{\star,i}$, is straightforward and implemented by a proportional controller of the form:

$$\begin{bmatrix} q_i^{glo} \\ r_i^{glo} \\ s_i^{glo} \end{bmatrix} = \mathcal{R}_2^{-1} \begin{bmatrix} \Phi_{\star,i} - \Phi_i \\ \Theta_{\star,i} - \Theta_i \\ \Psi_{\star,i} - \Psi_i \end{bmatrix}. \tag{37}$$

Thus, upon computation of (31b) and (32), control laws (36) and (37) are simultaneously activated. Upon achieving the desired position and orientation, control is handed back to local coverage mode if our guard condition $|\hat{e}_i(t)| \geq \varepsilon_1$ is satisfied. Otherwise, a full scan of $\mathcal{D}^j$ shall be conducted in scan coverage mode as elaborated upon in the proceeding section.

V. Scan Coverage Mode

The above strategies work very well for coverage of the vast majority of the domain. Agents effectively explore their immediate surroundings in local coverage mode and are intermittently redirected through global coverage to waypoints at which they may resume their active exploration. As $E(t) \to 0$, however, $|\hat{e}_i(t)|$ tends to be very small as the uncovered portions of the domain exist within numerous disconnected patches. This renders a gradient following technique, such as local coverage mode, to become less effective. Our past work, such as in [21], relied upon a persistent reactivation of global coverage mode. However, this is limited in that (31a) tends to select a different $\mathcal{D}^j$ upon each activation requiring the agents to spend substantial time relocating rather than completing the coverage of one single $\mathcal{D}^j$. Scan Coverage Mode addresses this problem by persistently selecting new orientations for agent i at $p_i = p_{\star,i}$ with $\mathcal{D}^{\tilde{j}}$ fixed until all $\tilde{p} \in \mathcal{D}^{\tilde{j}}$ are fully covered.

Note in Fig. 2 that scan coverage of $\mathcal{D}^j$ by i is initialized upon satisfaction of $G(\zeta_{i1}, \zeta_{i2})$. At this moment, a new optimal orientation, denoted $\Omega_{\star\star,i}$ is computed via (32) at the previous value for $p_{\star,i}$ selected in global coverage. Agent i's control laws under scan coverage are presented in our automaton vector field definition, $f(\zeta_{i2}, q_i)$, where $[q_i^{scn}\ r_i^{scn}\ s_i^{scn}]^T$ may be computed from the right hand side of (37) with the elements of $\Omega_{\star\star,i}$ substituted for those of $\Omega_{\star,i}$. As noted in the vector field definition, the linear velocity commands are zero. Note that $G(\zeta_{i2}, \zeta_{i0})$ allows for the resumption of local coverage at any point if $|\hat{e}_i(t)| \geq \varepsilon_1$. Otherwise, upon satisfaction of $G(\zeta_{i2}, \zeta_{i3})$ a clock variable t_h is initialized to zero and the agent remains in a hold state with zero control inputs. This hold state guarantees a finite time convergence of the global coverage error (see *Theorem 2*). After time $t_h^\star$ has passed, control is then handed back to scan coverage and $\Omega_{\star\star,i}$ is recomputed. Assuming that local coverage is not activated, this cycle will continue until full coverage of $\mathcal{D}^{\tilde{j}}$ at which point we have $\hat{C}_i^{\tilde{j}} = \infty$ and control is returned to global coverage. The aforementioned finite time convergence guarantee is formalized in *Theorem 2*.

Theorem 2: Full coverage of $\mathcal{D}$ is guaranteed in finite time; that is, there exists $t_f > 0$ such that $E(t_f) = 0$.

Proof: Recall from our automaton that so long as agent i operates in local coverage mode, $G(\zeta_{i0}, \zeta_{i1})$ guarantees $|\hat{e}_i(t)| \geq \varepsilon_1$ and thus $\dot{E}(t) < 0$ is upper bounded such that $\dot{E}(t) \leq -\varepsilon_1 < 0$. If the assumption of a non-zero bound on $\dot{E}(t)$ holds for $t < t_f$, then there exists t_f such that $E(t_f) = 0$.

Now assume that at time $0 < t < t_f$ this upper bound on $\dot{E}(t)$ is persistently violated. The result shall be a closed walk which may be defined as the sequence of edges $\left((\zeta_{i1}, \zeta_{i2}), ((\zeta_{i2}, \zeta_{i3}), (\zeta_{i3}, \zeta_{i2}))^+, (\zeta_{i2}, \zeta_{i1})\right)$ where $+$ denotes the Kleene plus operator. As $E(t) > 0$, $\mathcal{D}^{\tilde{j}}$ exists at t with the property that $\hat{C}_i^{\tilde{j}}$ takes on a finite value $\forall i \in N$. That is, there exists at least one point $\tilde{p} \in \mathcal{D}^{\tilde{j}} \mid Q(t, \tilde{p}) < C^\star$. Denote this point $\tilde{p}^\star$. The requirement that the $\ell \times \ell \times \ell$ cube $\mathcal{D}^{\tilde{j}}$ have the property that $\ell \leq \sqrt{2} R_i$ guarantees that there exists $q_i^{\star\star} = \left[p_{\star,i}^T\ \Omega_{\star\star,i}^T\right]^T \mid \tilde{p}^\star \in int(\mathcal{S}_i)$. Therefore, $S_i(q_i^{\star\star}, \tilde{p}^\star) > 0$. The hold state, which commands zero control input, guarantees that these conditions may be maintained for a time interval of length $t_h^\star$. $Q(t, \tilde{p}^\star)$, noting (6) and (7), increases linearly in time over this interval as $\mathcal{S}_i$ is stationary. This constant rate of change for $Q(t, \tilde{p}^\star)$ guarantees that there exists a sufficient number of these intervals such that $Q(t, \tilde{p}^\star) \geq C^\star$ at which point the set $\tilde{p}^\star$ is now empty and $\mathcal{D}^{\tilde{j}}$ is fully covered. The closed walk shall then start over with a new element from $\mathcal{D}^j$ selected as $\mathcal{D}^{\tilde{j}}$. The set $\mathcal{D}^j$ contains a finite number of elements and spans $\mathcal{D}$. Therefore, there exists some time t_f such that $Q(t, \tilde{p}) \geq C^\star\ \forall \tilde{p} \in \mathcal{D}$ implying $E(t_f) = 0$. This concludes

the proof. ■

VI. Simulations

A series of three simulations were performed to verify the efficacy of the algorithm. In all trials, three agents are deployed into a 200 x 200 x 100 cuboid which much be covered to a level of $C^\star = 0.5$. For each agent $i \in \{1, 2, 3\}$: $R_i = 10$, $r_i = 3.5$, $\Lambda_{i1} = 1$, $k_u^{loc} = k_v^{loc} = k_w^{loc} = 0.07, k_r^{loc} = k_s^{loc} = 0.015$, $\varepsilon_1 = 0.05$, $\varepsilon_2 = 0.1$, and $\varepsilon_3 = 0.01$. γ_{ik}, $\forall k \in \{1, ..., 5\}$, were chosen as the same value for each agent and is denoted as simply γ_i in this section. The evolution of the normalized coverage coverage error, normalized actuation effort, and inter-agent distances for each trial are presented in Fig. 3, 4, and 5 respectively. Note that inter-agent distances remain above $2r_i$; therefore, collision is avoided in all trials. Actuation effort, defined as $\int_0^{t_{gc}} |u_i(\tau)| + |v_i(\tau)| + |w_i(\tau)| + |r_i(\tau)| + |s_i(\tau)| d\tau$, is an integral of the time history of kinematic commands issued to an individual agent. This term is used to quantify the effects of our energy consumption cost weights γ_i, Λ_{i0}. Actuation effort is normalized to the highest value of any of the three trials (i.e., agent 2 in trial one for this set). Λ_{i1} remains fixed across all trials because only its magnitude relative to Λ_{i0} and γ_i affects the selection of $\tilde{j}$. Reducing Λ_{i0} and γ_i may be done in a manner equivalent to increasing Λ_{i1}.

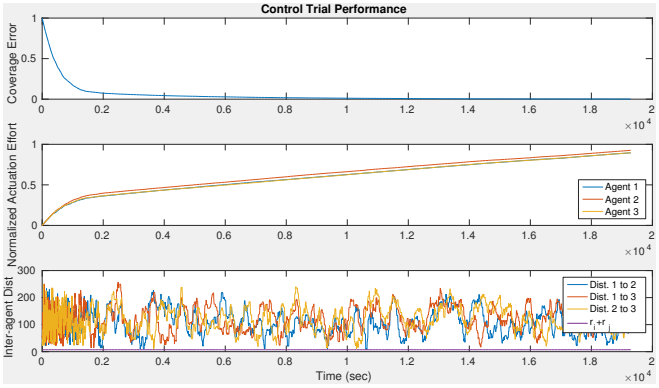

Fig. 3. For the control trial: $\gamma_1 = 0$, $\gamma_2 = 0$, $\gamma_3 = 0$, $\Lambda_{10} = 0.5$, $\Lambda_{20} = 0.5$, and $\Lambda_{30} = 0.5$.

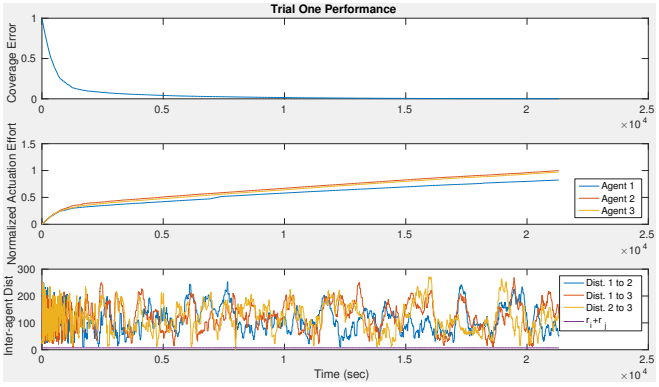

Fig. 4. For trial one: $\gamma_1 = 10^{-4}$, $\gamma_2 = 0$, $\gamma_3 = 0$, $\Lambda_{10} = 0.5$, $\Lambda_{20} = 0.5$, and $\Lambda_{30} = 0.5$.

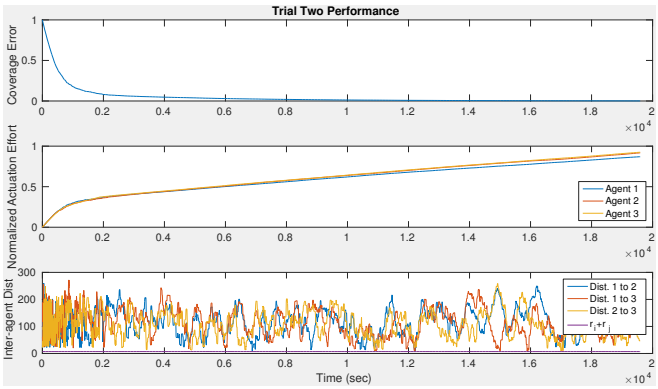

Fig. 5. For trial two: $\gamma_1 = 0$, $\gamma_2 = 0$, $\gamma_3 = 0$, $\Lambda_{10} = 1$, $\Lambda_{20} = 0.5$, and $\Lambda_{30} = 0.5$.

The control trial establishes a baseline for which no dynamic weights are utilized and the static weights are constant across all agents. The coverage error is reduced by 90% and 99.9% in 1,402 and 19,292 seconds respectively as evidenced in Fig. 3. The integrated actuation effort is relatively consistent between the three agents at 90%, 93%, and 90% of the peak value (i.e., agent 2 in trial one) respectively. To verify *Theorem 2*, the control trial was continued until 100% coverage, within a tolerance of 10^{-10}, was achieved at 27,398 seconds. The operating modes of each agent throughout the control trial are presented in Fig. 6. Fig. 3 and Fig. 6 illustrate that the first 2,000 or so seconds of coverage is characterized by a rapid reduction in the coverage error to less than 10% as the agents actively explore in local coverage mode. For many applications, this performance is sufficient. However, the final 10% of the domain may be explored through continual switches between global coverage and scan coverage at a diminished coverage rate. For reference, the trajectories of agents in the control trial are included in Fig. 7.

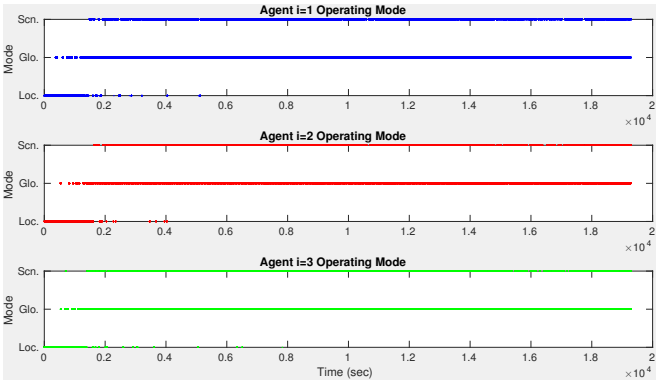

Fig. 6. Discrete states are presented for the control trial. Agents tend to remain in local coverage for the first 2,000 seconds with the remainder of time characterized by continual switches between global coverage and scan coverage. Note that the hold state is included in scan coverage.

In trial one, the coverage error is reduced by 90% and 99.9% in 1,846 and 21,308 seconds respectively at which point the simulation was terminated. A dynamic gain, $\gamma_1 =$

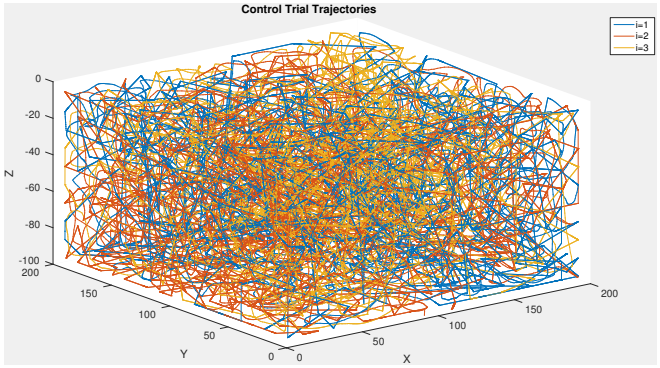

Fig. 7. Agent trajectories are presented for the control trial.

10^{-4}, was placed on agent 1 while the static weights were held constant across all agents. This reduced the actuation effort of agent 1 to 82% at the termination of coverage while agents 2 and 3 were at 100% and 97% of peak actuation effort respectively. In trial two, the coverage error is reduced by 90% and 99.9% in 1,722 and 19,594 seconds respectively at which point the simulation was terminated. The static gain of agent 1, Λ_{10} is increased from 0.5 to 1 in this trial with no dynamic gains. The cost savings for agent 1 in trial two are only marginally effective in that actuation efforts are 87%, 92% and 92% for the three agents respectively.

VII. Conclusions

This paper has presented an energy-aware 3D dynamic coverage control algorithm which extends the authors' previous studies in [20], [21]. This coverage strategy is novel in that it results in control laws applicable to a visually-based active 3D search/patrol protocol. This algorithm, particularly the local coverage strategy, may be easily extended to non-convex, geometrically elaborate domains. This facilitates active exploration in circumstances where preplanned paths are hard to obtain (e.g., ship wrecks, unfamiliar enemy territory, Martian caves, etc.). Previous work on this topic has been restricted to fixed cameras [15], [16] and quasi-3D coverage domains [17]. The efficacy of the algorithm has been demonstrated through a series of simulations which highlight the energy-saving effects of tuning the cost weights. Specifically, it was shown that a power constrained agent may be designated to cover the domain in a reduced capacity while the remaining agents compensate with little effect on the final coverage time.

Future work will explore the use of density maps and information decay to model persistent coverage of 3D dynamic environments.

References

[1] M. Abazeed, N. Faisal, S. Zubair, and A. Ali, "Routing protocols for wireless multimedia sensor network: A survey," *Journal of Sensors*, 2013.

[2] Y. Zhang, X. Li, J. Yang, Y. Liu, N. Xiong, and A. V. Vasilakos, "A real-time dynamic key management for hierarchical wireless multimedia sensor network," *Multimedia Tools and Applications*, vol. 67, no. 1, pp. 97–117, 2013.

[3] J. Cortes, S. Martínez, T. Karatas, and F. Bullo, "Coverage control for mobile sensing networks," *IEEE Trans. on Robotics and Automation*, vol. 20, no. 2, pp. 243–255, 2004.

[4] A. Kwok and S. Martínez, "Energy-balancing cooperative strategies for sensor deployment," in *Proc. of the 2007 IEEE Conference on Decision and Control*, New Orleans, LA, Dec. 2007, pp. 6136–6141.

[5] A. Kwok and S. Martinez, "Deployment algorithms for a power-constrained mobile sensor network," in *Proc. of the 2008 IEEE International Conference on Robotics and Automation*, Pasadena, CA, may 2008, pp. 140–145.

[6] C. Zhu, C. Zheng, L. Shu, and G. Han, "A survey on coverage and connectivity issues in wireless sensor networks," *Journal of Network and Computer Applications*, vol. 35, no. 2, pp. 619–632, 2012.

[7] J. Liang, M. Liu, and X. Kui, "A survey of coverage problems in wireless sensor networks," *Sensors and Transducers*, pp. 240–246, 2014.

[8] D. M. Stipanović, C. Valicka, C. J. Tomlin, and T. R. Bewley, "Safe and reliable coverage control," *Numerical Algebra, Control and Optimization*, vol. 3, pp. 31–48, 2013.

[9] I. I. Hussein and D. M. Stipanović, "Effective coverage control for mobile sensor networks with guaranteed collision avoidance," *IEEE Trans. on Control Systems Technology*, vol. 15, no. 4, pp. 642–657, Jul. 2007.

[10] B. Liu, O. Dousse, P. Nain, and D. Towsley, "Dynamic coverage of mobile sensor networks," *IEEE Transactions on Parallel and Distributed systems*, vol. 24, no. 2, pp. 301–311, 2013.

[11] N. Hübel, S. Hirche, A. Gusrialdi, T. Hatanaka, M. Fujita, and O. Sawodny, "Coverage control with information decay in dynamic environments," in *Proc. of the 17th IFAC World Congress*, Seoul, South Korea, Jul. 2008, pp. 4180–4185.

[12] P. Hokayem, D. Stipanovíc, and M. Spong, "On persistent coverage control," in *Proc. of the 2007 IEEE Conference on Decision and Control*, New Orleans, LA, USA, Dec. 2007, pp. 6130–6135.

[13] C. Song, L. Liu, G. Feng, Y. Wang, and Q. Gao, "Persistent awareness coverage control for mobile sensor networks," *Automatica*, vol. 49, no. 6, pp. 1867–1873, 2013.

[14] S. Oktug, A. Khalilov, and H. Tezcan, "3D coverage analysis under heterogeneous deployment strategies in wireless sensor networks," in *Proc. of the 2008 Fourth Advanced International Conference on Telecommunications*, 2008, pp. 199–204.

[15] C. Piciarelli, C. Micheloni, and G. L. Foresti, "Automatic reconfiguration of video sensor networks for optimal 3D coverage," in *Proc. of the 2011 Fifth ACM/IEEE International Conference on Distributed Smart Cameras (ICDSC)*, 2011, pp. 1–6.

[16] L. Xie and X. Zhang, "3D clustering-based camera wireless sensor networks for maximizing lifespan with minimum coverage rate constraint," in *Proc. of the 2013 IEEE Global Communications Conference (GLOBECOM)*, 2013, pp. 298–303.

[17] P. Cheng, J. Keller, and V. Kumar, "Time-optimal UAV trajectory planning for 3D urban structure coverage," in *Proc. of the 2008 IEEE/RSJ International Conference on Intelligent Robots and Systems*, Nice, France, Sep. 2008, pp. 2750–2757.

[18] M. Cardei and J. Wu, "Energy-efficient coverage problems in wireless ad-hoc sensor networks," *Computer Communications*, vol. 29, pp. 413–420, 2006.

[19] X. Wang, S. Han, Y. Wu, and X. Wang, "Coverage and energy consumption control in mobile heterogeneous wireless sensor networks," *IEEE Trans. on Automatic Control*, vol. 58, no. 4, pp. 975–988, 2013.

[20] D. Panagou, D. M. Stipanović, and P. G. Voulgaris, "Distributed dynamic coverage and avoidance control under anistropic sensing," *accepted as Full Paper in IEEE Transactions on Control of Network Systems, to appear*.

[21] W. Bentz and D. Panagou, "An energy-aware redistribution method for multi-agent dynamic coverage networks," in *Proc. of the 2016 IEEE Conference on Decision and Control*, Las Vegas, NV, Dec. 2016.

[22] R. W. Beard, "Quadrotor dynamics and control," 2008, lecture notes.

[23] J. Lygeros, "Lecture notes on hybrid systems," 2004, eNSIETA course, https://pdfs.semanticscholar.org/2a63/e3e98264ee40ae76a933ad8d7ea0ee7033d5.pdf.

[24] J. C. Slattery, *Advanced Transport Phenomena*. Cambridge UP, 1999.

[25] D. Panagou, D. M. Stipanović, and P. G. Voulgaris, "Distributed coordination control for multi-robot networks using lyapunov-like barrier functions," *IEEE Transactions on Automatic Control, to appear*, vol. 61, no. 3, pp. 617–632, Mar. 2016.

[26] X. Ma, Z. Jiao, Z. Wang, and D. Panagou, "Decentralized prioritized motion planning for multiple autonomous UAVs in 3D polygonal obstacle environments," in *2016 International Conference on Unmanned Aircraft Systems (ICUAS)*, June 2016, pp. 292–300.

[27] A. G. Wills and W. P. Heath, "A recentred barrier for constrained receding horizon control," in *Proceedings of the 2002 American Control Conference*, May 2002, pp. 4177–4182.